ecologies

MDPI

Article

Rapid Estimation of Mangrove Area and Carbon Sequestration in Land Subsidence Regions of Coastal Taiwan

Feng-Jiau Lin [1], Shu-Hui Chang [2], Cheng-Wei Lin [1], Kuan-Feng Huang [3], Hsiao-Yun Chang [4] and Yih-Tsong Ueng [2,*]

[1] Tainan Hydraulics Laboratory, National Cheng Kung University, No. 500, Section 3, Anming Rd., Annan Dist., Tainan City 70955, Taiwan; fjlin@mail.ncku.edu.tw (F.-J.L.); n8897106@mail.ncku.edu.tw (C.-W.L.)
[2] Department of Environmental Engineering, Kun Shan University, No. 195, Kunda Rd., Yongkang Dist., Tainan City 71003, Taiwan; tnisabel380817@gmail.com
[3] Bureau of Agriculture, Tainan City Government, No. 36, Min-Chih St., Xinying Dist., Tainan City 73001, Taiwan; beancrown@mail.tainan.gov.tw
[4] Department of Medical Laboratory and Biotechnology, Asia University, No. 500, Lioufeng Rd., Wufeng, Taichung 41348, Taiwan; chuan@asia.edu.tw
* Correspondence: ytueng@gmail.com; Tel.: +886-995965928; Fax: +886-62050540

Abstract

Mangrove ecosystems along Taiwan's southwest coast have been increasingly stressed by climate change, subsidence, and sea level rise. Between 1897 and 2024, the mean annual temperature rose by 2.0 °C, and rainfall declined by 56.5 mm. Severe subsidence occurred in Taixi Township, Yunlin County (−283.0 cm, 1975–2023), where the gray/white mangrove (*Avicennia marina*) exhibited reduced growth and mortality. Long-term mangrove area (MA) was reconstructed using quadratic polynomials: Tougang Ditch, $MA_{TG}(t) = -0.0084(t - 21.0)^2 + 2.8$ peaking in 1995 ($R^2 = 0.7274$), and Budai Lagoon, $MA_{BD}(t) = -0.0468(t - 12.3)^2 + 26.1$ peaking in 1986 ($R^2 = 0.782$). Both sites yielded moderate fits indicating partial but less reliable reconstruction. In contrast, Jishui Estuary subsites displayed distinct maxima with stronger fits ($R^2 > 0.85$): JS-C, $MA_{JS\text{-}C}(t) = -0.0201(t - 14.3)^2 + 7.0$ peaking in 1996; JS-D, $MA_{JS\text{-}D}(t) = -0.0093(t - 15.8)^2 + 2.2$ peaking in 1998; and JS-G, and $MA_{JS\text{-}G}(t) = -0.0077(t - 11.6)^2 + 4.3$ peaking in 1994. SPOT-6 satellite imagery (22 February 2025) identified 281.9 ha of mangrove and windbreak forests in Chiayi County and 896.3 ha in Tainan City. By integrating climate records, subsidence data, sea level rise, polynomial modeling, and satellite observations, this study provides a robust framework for anticipating mangrove trajectories, assessing carbon sink potential, and refining carbon credit estimates in vulnerable coastal landscapes.

Keywords: *Avicennia marina*; blue carbon; climate change; sea level rise; annual ring-width; trend analysis

Check for updates

Academic Editor: José Ramón Arévalo Sierra

Received: 29 December 2025
Revised: 4 February 2026
Accepted: 9 February 2026
Published: 13 February 2026

Copyright: © 2026 by the authors. Licensee MDPI, Basel, Switzerland. This article is an open access article distributed under the terms and conditions of the Creative Commons Attribution (CC BY) license.

1. Introduction

1.1. Implications of Climate Change

Taiwan has a tropical climate characterized by distinct wet and dry seasons, with a rainy summer (April–September) and a dry winter (October–March). Rainfall during the wet season is approximately ten times that during the dry season, and annual rainfall fluctuates considerably [1]. During the rainy season, freshwater input reduces salinity, thereby enhancing photosynthesis and growth, resulting in higher leaf area index values compared to the dry season [2]. However, runoff also transports sediments and organic

matter into coastal zones where mangroves grow [3,4]. In some regions, the semiannual rainfall is strongly correlated with mangrove radial growth (correlation coefficient: >0.9) [4], and similar rainfall–growth associations have been observed in other areas. Rainfall is also associated with annual ring width in red mangrove (*Rhizophora mangle*) [5], black mangrove (*Avicennia germinans*) [6], and even in planted white spruce (*Picea glauca*) [7]. This rainfall–growth relationship corresponds to a net primary productivity of 8.82 g of carbon per square meter per day [8].

1.2. Mangroves

Mangroves are plant communities that grow in intertidal zones of tropical and subtropical estuaries, lagoons, and bays [9–11]. These salt-tolerant species enrich estuarine environments by facilitating nutrient exchange and deposition through river flow and tides [12–15]. Beyond their high productivity and role in maintaining ecological balance, mangroves are critical for environmental protection. They offer essential habitats for birds, benthic organisms, and fish, such as juveniles of *Lutjanus cyanopterus* [16–18]. These plants support abundant benthic organisms, facilitating the formation of a complete food web [17–20]. Furthermore, mangroves maintain the stability and diversity of fish communities [12,21–24], thereby supporting fishery resources. Studies have revealed that the distributions of large, medium, and small fish were 18.2%, 24.2%, and 57.6%, respectively, including 32 fish species listed in the International Union for Conservation of Nature Red List [2,24].

1.3. Changes in Taiwan's Mangrove Landscape

Comprehensive surveys have revealed changes in the area, species composition, and diversity of Taiwan's mangroves that have occurred over time [19,25]. Mangrove area (MA) in 37 major distribution regions increased slowly from 178 ha in 1966 to 226 ha in 1986 and then rapidly to 586 ha between 1986 and 2011; of the total MA, the area covered by the gray/white mangrove *Avicennia marina* was approximately 320 ha [19,26,27]. Taiwan currently has approximately 681 ha of mangroves, which constitute major ecosystems and blue carbon sources in coastal regions [11,27,28].

Mangroves provide habitats for prawns (e.g., *Exopalaemon carinicauda*), crabs (e.g., *Metaplax elegans*), and fishes (e.g., *Gerres erythrourus*), shellfish (e.g., *Fronsella taiwanica*) [29]. Large mangrove stands in southwest Taiwan's Danshueih, Puzih, Jishui, Cigu, and Yanshuei estuaries often attract egrets to nest and breed [30–33]. Mature mangrove forests harbor diverse insects and spiders [29,34,35] and serve as carbon sinks across regions [36–39].

1.4. Land Subsidence

Climate change is causing the sea level to rise. Additionally, research has revealed global land subsidence due to groundwater overpumping in Egypt [40]. In Taiwan, coastal land formed within the last 300 years is more prone to over-extraction of groundwater and subsidence [37,39]. The causes of mangrove destruction vary across regions. For example, in other area, Villate Daza et al. reported that the 40,000 hectares of mangroves in the Caribbean Sea of Colombia were lost due to coastal erosion, urban expansion, altered forest hydrology, and illegal logging [6]. Mining activities in New Zealand have also contributed to coastal degradation and mangrove decline [20]. The ascending respiratory roots of *A. marina* are often submerged in seawater. Tropical and subtropical regions that support winter growth of *A. marina* now face land subsidence at rates exceeding sea level rise [21], particularly in South Asia, Southeast Asia, and East Asia [39–41]. In Zhuhai, China, the maximum annual subsidence rate has reached −11.0 cm [20,41–44]. Taiwan's western plain, formed within the last three centuries [37], faces severe subsidence due to groundwater extraction for aquaculture. In Pingtung County, the average annual land subsidence rate

along the Linbian River was −18.4 cm from 1966 to 1983, and −4.5 cm from 1994 to 2024, resulting in a cumulative subsidence of −590 cm 1966 to 2024 [45,46]. Such extensive subsidence has led to recurring property losses during heavy rainfall.

1.5. Effects and Assessment of Land Subsidence in Coastal Taiwan

Large areas of *A. marina* originally existed at Dongshih Lagoon (DS) in Taiwan's Chiayi County. Between 1962 and 1963, the county government introduced *Kandelia obovata* mangroves from the Tamsui River, Taipei [47]. In 1963 and 1964, approximately 110 ha mangroves of *A. marina*, *A. officindlis*, and *Rhizophora conjugatam*, respectively, were introduced at Cigu Lagoon, Tainan City (Appendix A) [47]. However, Dongshih has been facing land subsidence since 1970. In 1988, the total MA in this region was only approximately 51 ha [48]. By 1990, *A. marina* mangroves along the coast of the Xingcuoliao and Xinjiezhuang villages had sunk or died due to land subsidence (Figure 1) [6,26,49]. If this pattern continues, mangroves may subsequently re-establish at displaced sites [50].

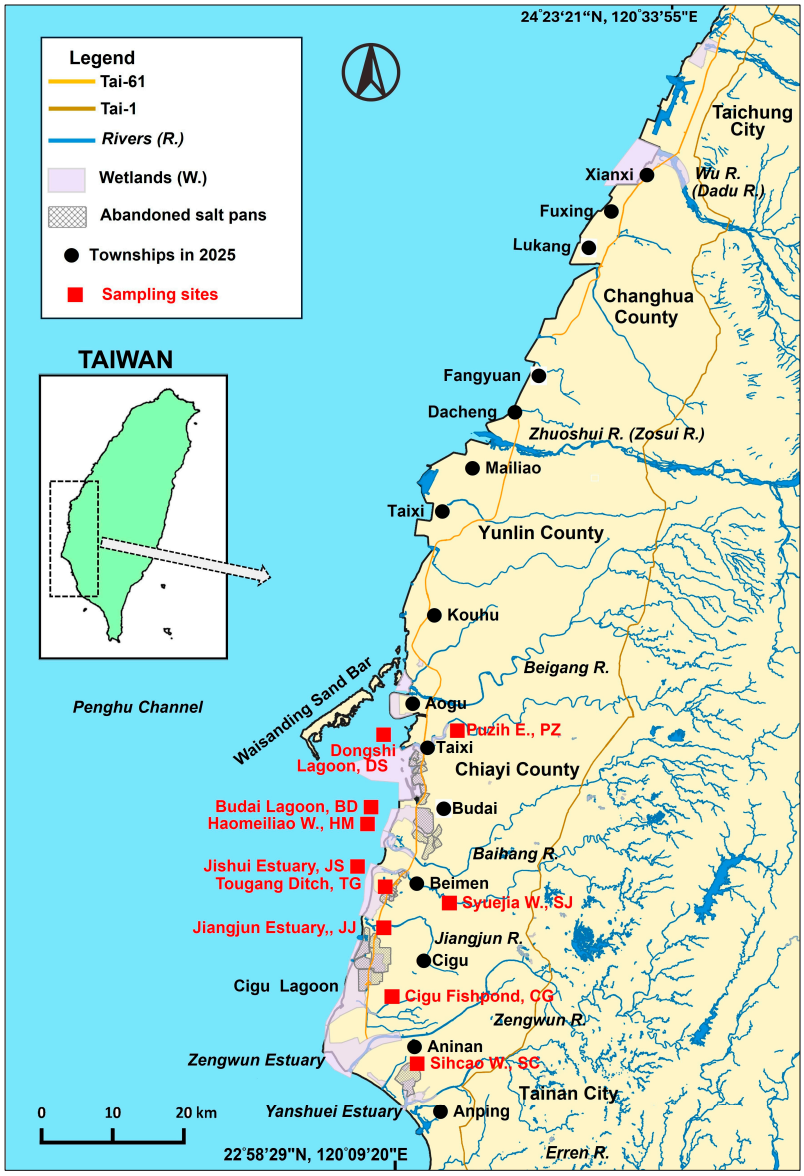


Figure 1. Research sampling sites of *Avicennia marina* in subsiding coastal estuaries and river systems along western Taiwan.

Originally, DS was covered with approximately 40 ha of *A. marina*. The Puzih Estuary (PZ; Chiayi County) contained 3 ha of *K. obovata* and *A. marina*, Budai Lagoon (BD, Chiayi County) had 30 ha of *A. marina*. The Jishui Estuary (JS) and Tougang Ditch (TG) in Tainan City encompassed 50 ha of mixed mangroves, including *A. marina*, *K. obovata*, *L. racemosa*, and *Excoecaria formosana* [11,12,49,51].

In 1975, the mangrove forests at JS were dominated by *A. marina*, with very few *L. racemosa*, *K. obovata*, and *E. formosana*. Initially, the south bank was not subjected to seaside development or embankment reconstruction. The seaside was developed in 1989, and the embankment was reconstructed in 2009. Reconstruction of embankments or redirection of water flow resulted in varying degrees of erosion or siltation in river-mouth mudflats, modulating changes in MA. In 1975, the Water Resources Agency under the Ministry of Economic Affairs initiated monitoring of land subsidence along Taiwan's west coast to assess long-term impacts arising from groundwater overpumping [52,53]. Geographic information system technology and satellite imagery have since been used to analyze changes in MA [54,55]. The compounding effects of climate change are analyzed by incorporating relative increase in sea level, defined as the sum of land subsidence and sea level rise [56].

1.6. Mangrove Productivity and Carbon Sequestration

In India, *A. marina* has high growth efficiency and biomass yield. Its carbon stock (t/ha) is 75% higher than that of local *R. mucronata* and 3–8 times higher than that of *A. marina* in Taiwan [11]. Fan evaluated annual litterfall in mangroves and sea sedge at JS between October 2002 and September 2004, reporting total annual mangrove litterfall values of 11.78 and 12.55 Mg/ha/year, respectively [12,57]. Another study found that the average net photosynthetic rate of *A. marina* in Taijiang National Park was 4.87 μmol/m^2/s [58]. Li (2015) further reported that the annual carbon storage of sea sedge at Cigu Wetland and Sihcao Wetland (SC) was 12.64 Mg C/ha/year, with a net ecosystem production was 5.83 Mg C/ha/year (46.1%) [59]. Wu reported annual carbon storage of *A. marina* in Fangyuan, Budai, Beimen, and Cigu, with net production rates of were 15.67, 10.002, 7.08, and 12.64 Mg C/ha/year, respectively [37]. The carbon storage of Budai and Beimen were only 77.6% and 58.1% higher than that in Cigu and Sihcao. Wu attributed the low net production of *A. marina* at Budai and Beimen to their proximity to the estuary [37], whereas Chang linked low net production at Puzi and Beimen mainly to land subsidence [4]. Severe subsidence reduced the annual growth radius of *A. marina* and led to gradual mortality [4]. These inconsistent conclusions highlight the need for further research across with varying subsidence levels. In the present study, we examine the implications of climate change and the adaptive responses of *A. marina* by analyzing long-term changes in annual ring width and MA.

2. Methods

2.1. Study Sites

Between 2009 and 2025, nine sampling sites along Taiwan's west coast—from the Beigang River in Chiayi County to the Jiangjun River in Tainan City—panned approximately 100 km. Analysis was performed in two phases. During the first phase (2009–2012), sampling was carried out at DS (23.48163° N, 120.14454° E) and BD (23.36710°E, 120.14877° N), where mangroves have been recently dead for many years [26,48], as well as JS (23.24360° N, 120.09461° E) and Tougang Ditch (TG; 23.27696° N, 120.12039° E), where mangroves had recently died. Additional sites included SC (23.03181° N, 120.14703° E) and Jiangjun Estuary (JJ; 23.22543° N, 120.11598° E), representing areas with varying degrees of land subsidence: (Figure 1).

DS lies south of the Beigang River, Liujiao Ditch, and Aogu Wetland. It contains shallow waters protected to the west by Waisanding Sand Bar. Notably, DS is a key oyster farming area in Chiayi County. Here, *A. marina* mangroves were planted in 1962–1963, but they have disappeared because of severe land subsidence [7,28].

BD is located on the south side of Budai Harbor in Chiayi County and on the west side of the West Coast Expressway. It is another key oyster culture area in Chiayi County. The lagoon previously hosted *A. marina* mangroves, but they have disappeared because of land subsidence.

JS extends from the estuary to Wuwang Bridge. Historically, it supported abundant *Sanguinolaria diphos* (Bivalvia) and served as an egret roosting site. Mangroves at JS are dominated by *A. marina*, with *L. racemosa*, *K. obovata*, *E. formosana*, and *Volkameria inermis* scattered along the southern coast; some *A. marina* may develop pendent roots to protect itself before dying [4]. Mangroves are considered important species in estuarine ecosystems in various regions and are protected; trees are not easily cut down. In spring 2011, 10 mangrove tree samples were collected from JS, after which the remaining trees gradually died (Figure 2). TG is a tributary of the Jishui River. In spring 2011, 10 dead tree samples were collected from TG (Figure 2).

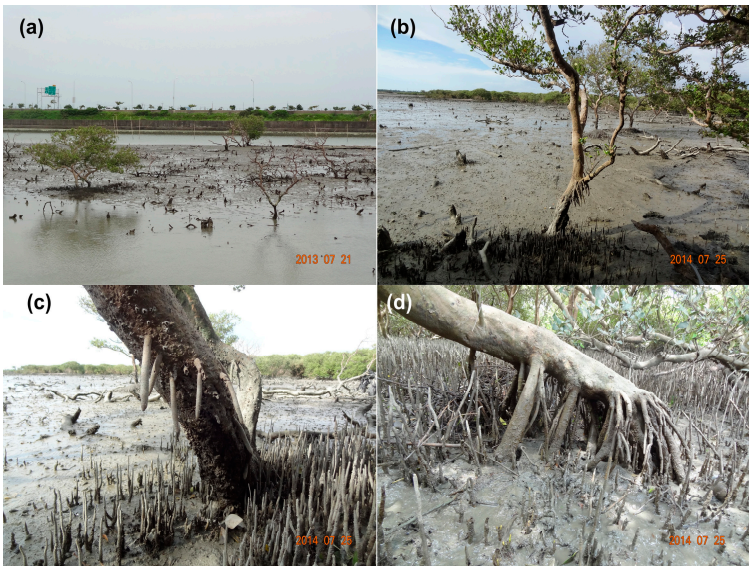


Figure 2. *Avicennia marina* mangrove in habitats prone to land subsidence at Tougang Ditch (TG) (**a**) and Jishui Estuary (JJS) (**b**–**d**). Showing large numbers of dead *A. marina* mangroves in TG and JS, the downward pendent roots (**b**,**c**), and pendent roots touching the mudflats (**d**).

The Jiangjun River lies between the BM and CG sites and flows into Beimen Lagoon. Its riverbanks are covered with *K. obovate* and *E. formosana*, as well as water lilies that have drifted in from elsewhere. After the river was cleaned up, some of the woodland was isolated in the low-lying areas outside the embankment.

SC is located on the west coast of Taiwan, where slight land subsidence occurs, and was included as the reference site. Mangroves grew at SC after construction of the West Coast Highway (Tai-17) and subsequent industrial zone development. Notably, mangroves at SC were used to infer the timing of mortality for those at TG. In spring 2011, four living mangrove trees were collected from SC.

The second phase (2023–2025) encompassed four sampling sites characterized by relatively low rates of land subsidence: PZ (23.47840° N, 120.19535° E) and Haomeiliao Wetland (HM, 23.36400° N, 120.13357° E) in Chiayi County as well as Syuejia Wetland (SJ; 23.27752° N, 120.16749° E) and JJ in Tainan City (Figure 1).

2.2. Subsampling Sites at JS

Not all mangroves were removed during the reconstruction of Jishui River embankment. Some mangroves in this area disappeared because of land subsidence [4,52,53]. To capture spatial variation, the JS site was divided into seven small subsites (JS-A–JS-G). JS-A has a spur where a new beach area forms annually. JS-B lies behind a dike constructed between 1989 and 2002, which encloses mangroves. In this period, a tidal ditch was demolished, the mangroves were removed, and fishponds were established. JS-C is adjacent to fishponds, while JS-D and JS-G are near the tidal zone. JS-F was formed by enclosing part of the Beimen Salt Pan in the waterway during dike reconstruction. A tidal channel lies between JS-G and JS-F (Figure 3). In the present study, areas disturbed because of dike construction were separated as much as possible. MAs of the seven sites were calculated for the period from 1975 to 2012. In addition, a carbon sink attenuation curve was generated for *A. marina* at the site with relatively low land subsidence.

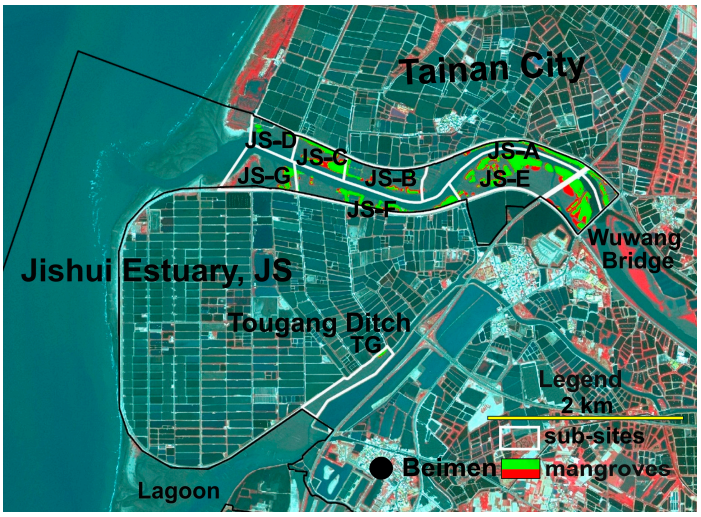


Figure 3. Map depicting Jishui Estuary (JS), Tougang Ditch (TG), and seven subsites within Jishui Estuary (JS-A–JS-G). The red and green areas within the range represent mangroves from different years.

2.3. Study Overview

All *A. marina* samples were sawed off from tree trunks close to the roots and brought to our laboratory at Kun Shan University. For each tree, the growth rings were measured during the dry and wet seasons each year, with a precision of 0.01 mm. The measurements for each tree were compiled into individual series. Annual ring width as [$YR_{s,i}(X)$], where s denotes the site, i the tree's serial number, and *X* the year, incorporating both wet-season and dry-season values. The series was used to estimate tree age, determine average annual ring width for each site and year, and construct the mean [$YR_S(X)$] series representing site-level growth dynamics.

2.4. Analysis of Long-Term Climate Data

Annual and monthly rainfall and average temperature data (1897–2024) were collected from the Former Tainan Meteorological Station (TN) [1]. Long-term (LT) climate trend models were applied [60,61]:

Linear trend of annual average temperature equation

$$T_{LT}(X) = aX + b \quad (1)$$

where a and b are constants and X denotes the year (1–128, corresponding to AD 1897–2024). (Unit: °C).

Linear trend of annual rainfall equation

$$P_{LT}(X) = aX + b \quad (2)$$

where a and b are constants and X denotes the year (1–128, corresponding to AD 1897–2024). (Unit: mm/year).

To reduce confusion caused by jagged line graphs, dynamic mean smoothing was applied [4,62–64]. The rainfall dynamic time-series sequence for Tainan (N = 19) was calculated as follows:

Annual rainfall dynamic time-series sequence (N = 19)

$$P_{TS}(X) = Avg[(P(X - 18) + \ldots + P(X))] \quad (3)$$

where X = 19–128 corresponding to AD 1915–2024. (Unit: mm/year).

Annual rainfall dynamic time-series sequences were analyzed to assess long-term fluctuations in precipitation. The period from April to September constitutes the wet season in Tainan, Taiwan (average monthly rainfall > 70 mm), whereas that from October to March constitutes the dry season (average monthly rainfall < 70 mm).

The half-year rainfall series sequence of TN was denoted as HP(TN,X). Alternating wet and dry half-year periods exerts cyclical [64] and staggered effects on plant growth, including a half-year radial growth rate and MA dynamics. The half-year rainfall dynamic time-series sequence (N = 2) was calculated as

$$HP_{TN}(X) = (HP(TN,X - 1) + HP(TN,X))/2 \quad (4)$$

where X = 2–79 corresponds to the months of October 1977 to October 2010. (Unit: mm/half-year).

Plant biodiversity is often lost under unsuitable climate conditions (e.g., temperature, rainfall, and conductivity) and altered land-use scenarios [65]. These stressors not only reduce biodiversity but also slow plant growth and compromise carbon capacity [4]. Rainfall delivers nutrients from the upstream catchments and lowers estuarine salinity, thereby enhancing photosynthesis, accelerating mangrove growth, and increasing trunk ring width [2,14]. In Taiwan, the frequency of extreme events has shifted markedly: wet years now occur once every 7 years instead of once every 19 years, while droughts occur once every $\leq$9 years instead of once every 17 years [66]. These shifts indicate that Taiwan is increasingly vulnerable to extreme weather events, with significant implications for ecosystem resilience and carbon storage.

By measuring the annual increase in the ring radius of 24 mangrove, we generated the matrix $[YR(X, S)]_{24\times37}$, where the row *X* indicates the year (1973–2010) and the columns indicate three study sites on Taiwan's west coast (JS, TG, and SC) and corresponding tree counts (4 to 10). Notably, some elements were blank.

The YR(X, S) series for each tree was compared with Tainan's annual rainfall data for the same period. Similarity analyses were performed using the Resemblance in PRIMER 7 [67]. To facilitate long-term dynamic analysis, the average value of YR(X,S) for trees at the same study site in the same year was calculated, yielding a new series that was subsequently examined using a quadratic polynomial trend equation, intersite differences in land subsidence, and subsidence outcomes. Similarity analysis was applied to evaluate the consistency between two sets of time series; a higher R^2 value indicates stronger agreement in their temporal dynamics.

2.5. Estimation of Land Subsidence

According to the Water Resources Agency, groundwater in coastal Taiwan has been overextracted to meet the demand of the rapidly expanding aquaculture industry [52]. This overuse has led to groundwater salinization and land subsidence. The most severely affected regions include Changhua, Yunlin, and Chiayi Counties and Tainan City in western Taiwan (Figure 1), as well as Pingtung County in the south and Yilan County in the north [52,53].

Monitoring data for the land subsidence were obtained from the Water Resources Agency for the following regions: Changhua County (N = 58, 1979–2023), Yunlin County (N = 95, 1975–2023), Chiayi County (N = 125, 1986–2023), and Tainan City (N = 84, 1987–2023). Records were compiled through 2023. Where annual data were missing, values were imputed using the internal-difference method. Notably, data for Beimen District in Tainan City followed the same monitoring schedule that was applied in Chiayi County. The monitoring data were analyzed to identify the effects of land subsidence on mangrove growth rates and coverage areas.

2.6. Estimation of MA for the Period from 1975 to 2025

The literature describes mangrove distributions across years, offering time-series data for mapping mangroves and estimating MA [4,68]. In the present study, we assessed changes in MA by using the following maps: (1) the 1975 Orthophoto Map from the Aerial Survey Office of the Ministry of Agriculture; (2) 1:5000 aerial photographs from 1983, 1989, 1991, 2002, 2009, and 2012, collected from the Aerial Survey Office, and the 1:5000 Taiwan Digital Map, prepared by the Van and referenced to aerial color orthoimages from the Aerial Survey Office; (3) the 2007 Google Map; and (4) SPOT-7 images from 22 March 2017, and 13 January 2023, and SPOT-6 images from 22 February 2025. These datasets covered the entire west coast of Taiwan.

For data conversion, the 1:5000 photograph-based map (paper) was purchased from the Agricultural and Forestry Aerial Survey Institute and subsequently scanned into a .tif file (Appendix B). It was digitized into a Taiwan Datum 1997 (TWD97) coordinate system by using the Georeferencing function in Esri ArcGIS 10.8 (Appendix C) [66,68–71].

Finally, the mangrove cover matrix in each study area was calculated as MA(S,t), where *S* is the site and *t* is the time: 1–43, representing December 1975–2017.

2.7. Estimation of Annual Ring Width in Mangroves

2.7.1. Estimation of Half-Year Ring Width Dynamic Time-Series Sequences

In spring 2011, samples were collected from 10 trees at JS and 4 trees at SC. TG contained 10 dead and leafless *A. marina* trees (total: 24 trees). Trunk samples collected near the roots were transported to the laboratory, cross-sectioned, and analyzed to construct time-series sequences of radius growth dynamics for the dry and wet seasons. These sequences are expressed as HG(S,X,i), where *S* represents the three study sites (TG, JS, and SC), *X* represents the half-year sequence (X = 1–79, corresponding to April 1972–April 2011), and *i* represents the tree code [8].

Many scholars have measured tree rings to estimate long-term annual rainfall, MA, biodiversity, nutrient intake, and carbon sequestration [7,66,71–75]. Some scholars have demonstrated that tree rings do not necessarily form once per year; some mangroves can produce 7 rings every 4 years [76,77]. To accurately identify the association between annual ring width and rainfall, we avoided radial lines that crossed $\geq$2 rings within a year when measuring the horizontal cross-sections of mangroves.

Because of the significant differences in growth between the dry and wet seasons [62], mangroves at TG either died or experienced severe decay. To accurately identify the

years in which *A. marina* died, we applied the permutation-order scale-invariant feature transform method and half-year growth ring widths. The best match between the two series was used to infer the lifespan of each *A. marina* tree that died. Average values for trees of the same age with known lifespan at TG site were then combined to construct a half-year radial growth dynamic time-series sequence, denoted as HG(TG,X). Ring widths were measured separately for the dry and wet seasons. The average half-year ring-width dynamic time-series sequence for *A. marina* (N = 2) is expressed as

$$[HG(S,X)] = (HG(TG,X-1,i) + HG(TG,X,i) \quad (5)$$

where X = 2–79 corresponds to half-year periods from October 1977 to October 2010. (Unit: mm/half-year).

The dynamic average half-year rainfall series sequence was denoted as $HP_{TN}(X)$. Five older/young *A. marina* trees were further used to construct another half-year radial growth time-series sequence, HG(TG-older, X) and HG(TG-young, X).

For each study site (JS, TG, SC), the annual ring width time series [$YR_S(X)$] was used to derive a quadratic trend line:

$$YR_S(X) = -k(X-p)^2 + q \quad (6)$$

where k, p and q are constants and X denotes the year (1–38; for example, at the TG site, AD 1973–2010). A negative value of −k indicated pronounced land subsidence, with the extremum q (mm/year) occurring in year p, corresponding to the peak (p, q) of the quadratic parabola. In contrast, a positive value of −k suggests no land subsidence or only minimal subsidence at the site S. The quadratic trend was further used to evaluate the consistency of movements between two sets of time series; a higher R^2 value reflects stronger agreement in their temporal dynamics (Appendix D). (Unit: mm/year).

2.7.2. Analysis of Long-Term Trends in MA

Using six sets of aerial images and two satellite images from 1975 to 2012, we obtained the long-term MA series, denoted as MA(S, t), where *S* represents DS, BD, JS, TG, or subsites JS-A–JS-G, and t = 1–37 corresponds to years AD 1975–2012. The quadratic polynomial trend equation for the long-term MA series is expressed as

$$MA_S(t) = -k(t-p)^2 + q \quad (7)$$

where k, p and q are constants and t denotes the year (1–38, corresponding to AD 1975–2012). (Unit: ha).

3. Results

3.1. Long-Term Changes in Annual Temperature and Rainfall

Climate records (1897–2024) from TN revealed average a monthly rainfall of 267.0 ± 145.2 mm during the wet season (April to September), and 27.0 ± 9.0 mm (range: 16.4–39.2 mm) during the dry season (October to March), indicating a clear seasonal contrast. The average annual temperature was 23.8 ± 0.7 °C (N = 128), which increased by 2.04 °C during the observation period and followed a long-term trend equation (Figure 4):

$$T_{LT}(X) = 0.0159X + 22.813 \ (R^2 = 0.7326)$$

where X = 1 corresponds to AD 1897 and X = 128 to AD 2024. (Unit: °C).

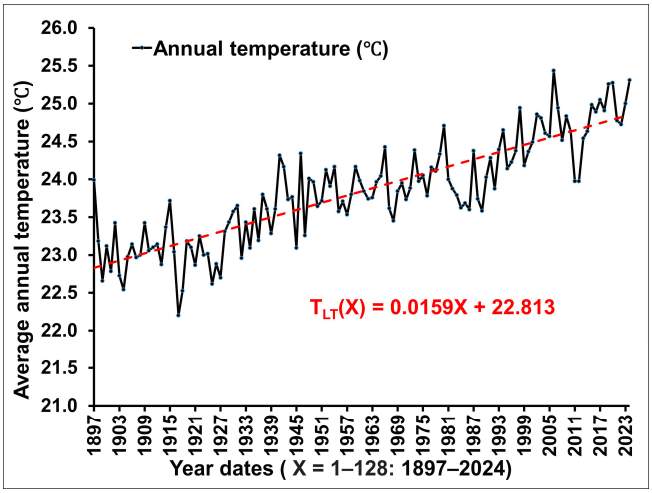


Figure 4. Changes in the long-term trend (T_{LT}) of annual temperature in Tainan. Data (1897–2024) were collected from the Tainan Meteorological Station.

The average annual rainfall was 1748.2 ± 532.1 mm. It decreased by 56.5 mm during the observation period and followed the long-term trend equation (Figure 5):

$$P_{LT}(X) = -0.4412X + 1776.7$$

where X = 1 corresponds to 1897 and X = 128 to AD 2024. (Unit: mm/year.)

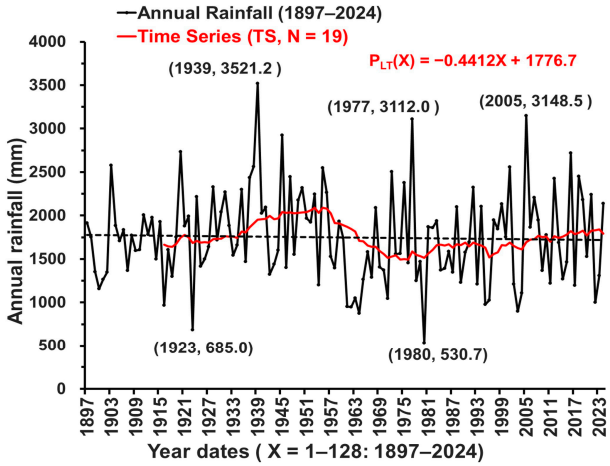


Figure 5. Changes in the long-term trend (P_{LT}) of annual rainfall in Tainan. Data (1897–2024) were collected from the Tainan Meteorological Station.

Time-series sequence (P_{TS}) analysis indicated that a wet period occurred approximately every 19 years; however, the last occurrence was in 1977. Subsequent intervals shortened and rainfall declined (Figure 5).

3.2. Land Subsidence Along the West Coast of Taiwan

Data (1975 to 2023) collected from the Water Resources Agency indicated extensive land subsidence from Shengang Township, Changhua County, southward to Annan District, Tainan City. The most severe subsidence occurred in Taixi Township, Yunlin County (−283.0 cm). In Chiayi County, Dongshih Township and Budai Township experienced subsidence of −233.6 cm and −179.4 cm, respectively. In Tainan City, Beimen District and Syuejia District recorded subsidence of −153.3 cm and −104.0 cm, respectively, during the same period (Figure 6).

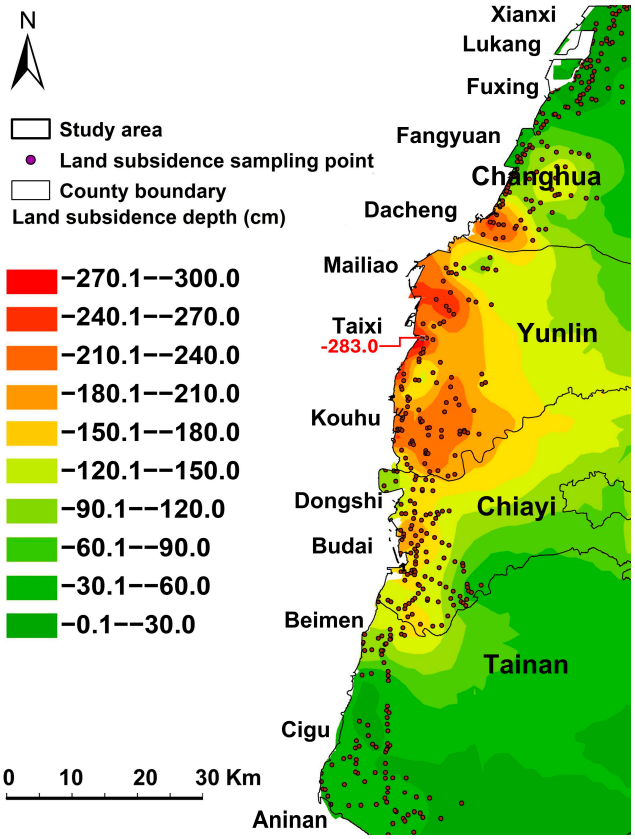


Figure 6. Land subsidence along the west coast of Taiwan. Data (1975–2023) were compiled from the Water Resources Agency, Ministry of Economic Affairs.

Among the three sites surveyed in 2009 and 2010, JS and TG were located in severely subsided areas. From 1975 to 2023, they experienced an average annual subsidence of −3.27 cm and −3.48 cm, respectively.

3.3. Changes in MA from 1975 to 2025

Orthophoto maps, 1:5000 aerial photographs, 1:5000 Taiwan Digital Map, Google Map, and SPOT-7 images from 22 March 2017, indicated that mangroves at DS, BD, JS, and TG were gradually disappearing or had completely disappeared. The MA across these four sites was 118.7 ha (Table 1). Mangroves at PZ expanded upstream to 77.6 ha (Appendix B Figure A1). After mangroves in the middle of BD died, only those near the windbreak of Haomeiliao Wetland on the inner side of the sandbar remained (Appendix B Figure A2). At JS, mangroves covered 17.5 ha, and by 2017, they had expanded upstream to SJ, reaching 23.3 ha (Appendix B Figure A3).

Table 1. Mangrove area along the southwest coast of Taiwan from 1975 to 2025 (ha).

Sampling Sites	Abbr.	1975	1983	1989	1991	2002	2009	2012	2017	2023
Dongshih Lagoon	DS	25.2	14.7	—	0.6	0				
Budai Lagoon	BD	14.6	35.5	26	—	6.3	0.4	0.3	0.1	
Jishui Estuary	JS	21.4	9.1	12.7	—	18.2	11.2	15.4	23.1	32.4
Tougang Ditch	TG	0	0.8	2.2	—	3.6	0.9	0.2	0.2	0.1
Total		61.2	60.1	40.9	—	28.1	12.5	15.9	118.7	32.5

Note: "—" indicates a lack of maps for corresponding years. Notably, it is already dead now because of land subsidence.

Spatiotemporal changes in MA along Taiwan's southwest coast from 1975 to 2017 were assessed using aerial images from 1975, 1983, 1989, 2002, 2009, and 2012. Subsequently, it declined due to the developing salt fields, the construction of Provincial Highway 61, and continual land subsidence. MA at BD was 14.6, 35.5, . . . and 0.0 ha; that of JS was 21.4, 9.9, . . . and 15.6 ha; and that of TG was 0.8, 2.2, . . . and 0.2 ha. MA across the DS, BD, JS, and TG sites increased from 61.2 ha in 1975 to 118.7 ha in 2017 (Table 2). JJ retained only 0.8 ha of *K. obovata* on the south bank because of extensive reclamation.

Table 2. Association between the *Avicennia marina* mangrove forest and land subsidence along the west coast of Taiwan.

Sites	AVG ± SD (mm)	Peak (mm)	Similarity to Annual Rainfall (%)	Max. of Trend Line	Year of Max.	Cumulative Subsidence (cm)	Annual Subsidence (cm/year)
TG	1.38 ± 0.39	1.94	78.4	1.759	1998	−153.3	−5.21
JS	1.04 ± 0.26	1.73	83.4	1.397	2022	−153.3	−4.34
SC	1.98 ± 0.34	2.5	81.0	2.179	2007	−47.5	−1.43

Changes in MAs at seven sites—DS, PZ, BD, HM, JS, TG, and SJ—between 1975 and 2017 are shown in Figure 7. The green areas indicate mangrove cover in 1975 that had disappeared by 2017. At the DS and BD lagoon sites, land subsidence reached approximately −230 cm and −180 cm, respectively, resulting in mangrove vanishing. At the PZ and JS estuaries sites, older mangroves died out, while new ones expanded upstream (Figure 7).

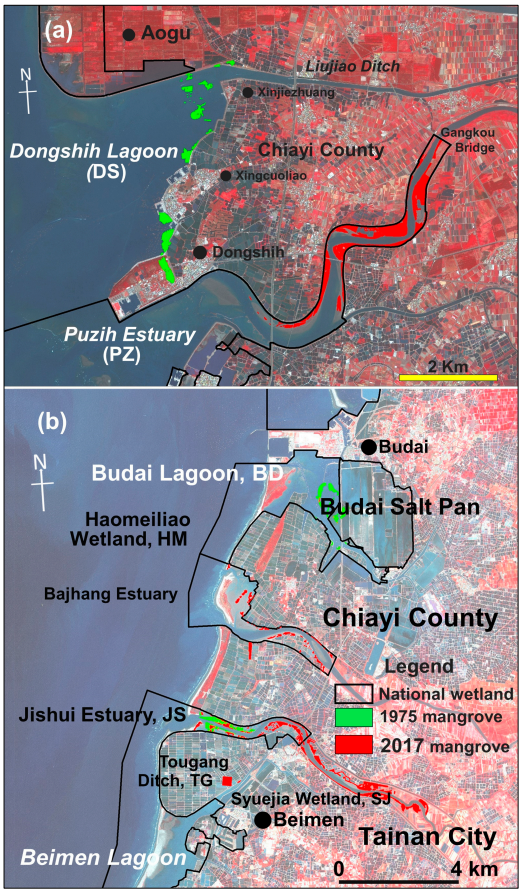


Figure 7. Changes in mangrove areas from 1975 to 2017: (**a**) Dongshih Lagoon (DS) and Puzih Estuary (PZ) in Chiayi County; (**b**) Budai Lagoon (BD) and Haomeiliao Wetland (HM) in Chiayi County, and Jishui Estuary (JS), Tougang Ditch (TG), and Syuejia Wetland (SJ) in Tainan City.

3.4. Long-Term Trends in MA

Based on the MA estimated from six aerial photographs and satellite images from 1975 to 2012, we performed a quadratic trend analysis of the MA series at TG. The equation was

$$MA_{TG}(t) = -0.0084(t - 21.0)^2 + 2.8 \ (R^2 = 0.7274)$$

where t = 1 corresponds to AD 1975 and t = 38 to AD 2012. (Unit: ha).

This result consistent with the time-series estimation of annual ring width. Quadratic polynomial trend analysis for BD site revealed the following equation:

$$MA_{BD}(t) = -0.0468(t - 12.3)^2 + 26.1 \ (R^2 = 0.782)$$

where t = 1 corresponds to AD 1975 and t = 38 to AD 2012. (Unit: ha).

At TG, the maximum MA occurred in 1995 (2.8 ha), whereas at BD, the maximum MA occurred in 1986 (26.1 ha; Figure 8).

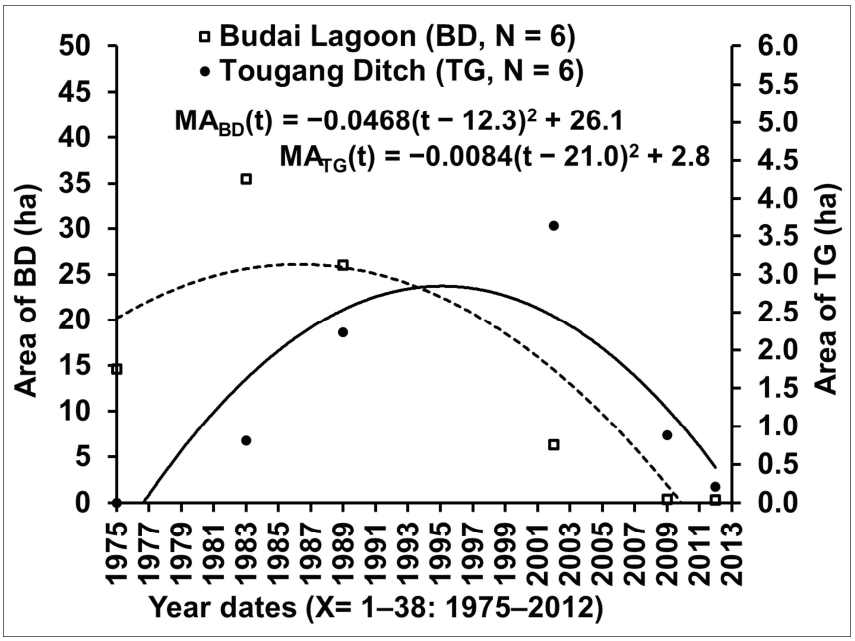


Figure 8. Vertex of the quadratic polynomial (estimated maximum value). Cumulative land subsidence for each study site.

At JS, MAs at subsites JS-A (new beach formed by diversion work) and JS-E (old salt beach incorporated into the river) increased exponentially, whereas those at JS-C, JS-D, and JS-G (three smaller sites near the river mouth) decreased. The results were as follows.

$$MA_{JS\text{-}C}(t) = -0.0201(t - 14.3)^2 + 7.0 \ (R^2 = 0.8554)$$

$$MA_{JS\text{-}D}(t) = -0.0093(t - 15.8)^2 + 2.2 \ (R^2 = 0.8956)$$

$$MA_{JS\text{-}G}(t) = -0.0077(t - 11.6)^2 + 4.3 \ (R^2 = 0.908)$$

At JS-C, JS-D, and JS-G, maximum MA occurred at t = 14.3 in 1996, t = 15.8 in 1998, and t = 11.6 in 1994, respectively. These peaks aligned closely with the maximum MA at TG in 1995 (Figure 9).

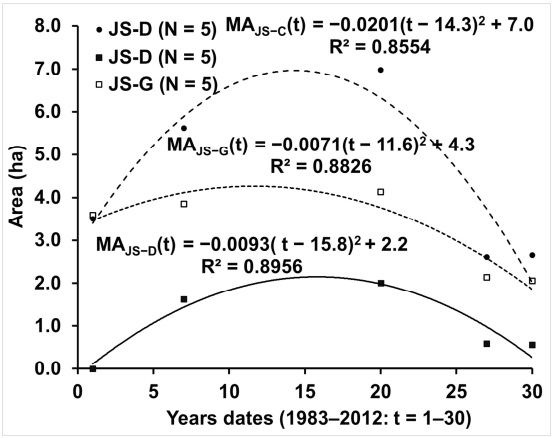


Figure 9. Changes in mangrove areas at Jishui Estuary subsites from 1983 to 2012.

3.5. MA in 2025

MA was estimated using SPOT 6 satellite images of the coastal area spanning the Beigang River in Chiayi County to the Jiangjun River in Tainan City, captured on February 22. The total MA and windbreak forest areas were 281.9 and 896.3 ha, respectively.

MA was the largest (109.1 ha) at the estuary of the Jishui River (including SJ and TG). The second-largest MA (85.4 ha) was at the mouth of Puzi Estuary (including the upstream section of Dongshih East Bridge). The third-largest MA (57.1 ha) was on the east side of Haomeiliao Sand Bar. Mangroves at Bajhang Estuary (including the channel south of the dike) covered 25.2 ha, whereas those at the Jiangjun River covered 4.9 ha. The Jiangjun River supported *K. obovata* and *E. formosana*. Windbreak forest area was the largest at Aogu (787.6 ha), followed by at Shuangchun (61.6 ha) and Jiangjun Estuary (47.1 ha; Figure 10).

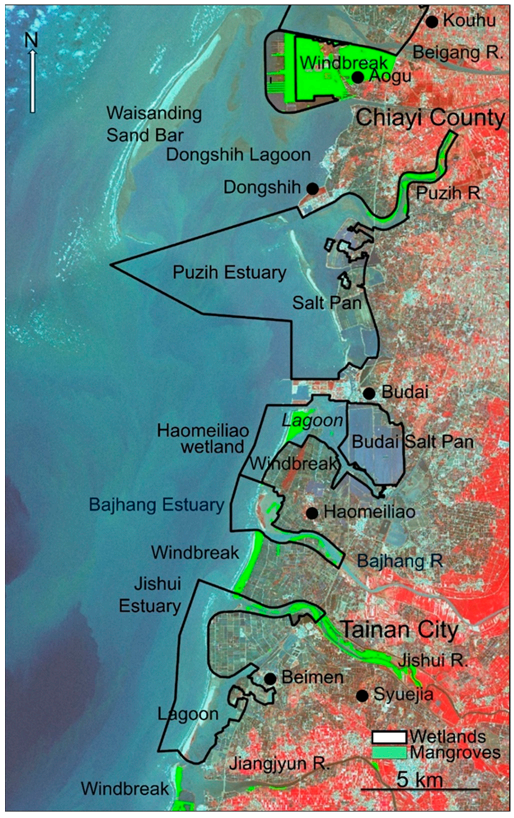


Figure 10. Distribution of mangroves and windbreak forests from the Beigang River (Chiayi County) to the Jiangjun River (Tainan City), based on data collected on 22 February 2025.

3.6. Annual Ring Width

In the first phase (2009–2012), similarity between average annual ring width and rainfall at TN was used to infer the age of each *A. marina* tree at TG. Lifespans were calculated from 1972 to 2008. The similarity between HG (TG-older, X) and HP(TN, X) was approximately 91%, whereas that between HG(SC, X) and HP(TN, X) was approximately 93%. The similarity between average annual ring width and annual rainfall was 80.0% at TG and 84.3% at JS. The annual ring width time series—$YR_{site}(X)$ values—for all *A. marina* trees across the SC, TG, and JS sites were combined and analyzed. The average annual ring width at SC was 1.98 ± 0.34 mm/year (N = 4), that at TG was 1.38 ± 0.39 mm/year (N = 10), and that at JS was 1.04 ± 0.26 mm/year (N = 10). The TG and JS were lower than those at SC.

3.7. Trends in Annual Ring Width and Land Subsidence

At TG, JS, and SC, the quadratic polynomial trend line equations of average annual ring width were:

$$YR_{TG}(X) = -0.002(X - 25.7)^2 + 1.716 \ (R^2 = 0.8233, N = 10)$$

$$YR_{JS}(X) = -0.0005(X - 38.5)^2 + 1.397 \ (R^2 = 0.559, N = 10)$$

$$YR_{SC}(X) = -0.0025(X - 17.6)^2 + 2.1736 \ (R^2 = 0.4189, N = 4)$$

The fastest annual radial increment occurred in 1998 at TG and in 2007 at JS (Figure 11). The average annual rates of land subsidence at TG, JS, and SC were −5.21, −4.34, and −1.43 cm, respectively (Table 2).

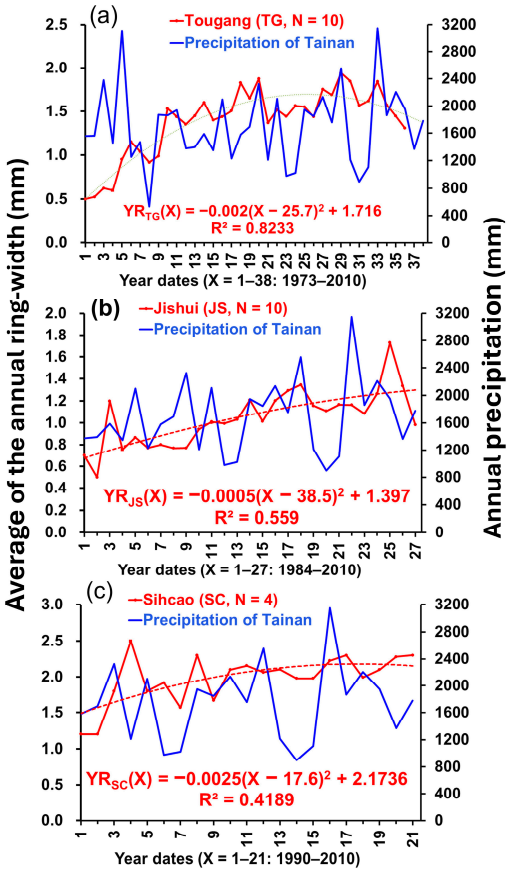


Figure 11. Estimate the time from prosperity to decline of mangrove forests in Tainan City: (**a**) Tougang Ditch (TG); (**b**) Jishui Estuary (JS); (**c**) Sihcao Wetland (SC).

Furthermore, at TG, the quadratic polynomial trend line equations of five older trees and five young trees' dynamic half-year ring width HG(S,X) were:

$$HR_{TG\text{-}older}(X) = -0.0003(X - 45.3)^2 + 0.7961 \ (R^2 = 0.7235, N = 5)$$

$$HR_{TG\text{-}youngr}(X) = -0.0008(X - 26.1)^2 + 0.9026 \ (R^2 = 0.6526, N = 5)$$

The largest increment for older trees occurred in 1995, whereas that for young trees occurred in 2002 (Figure 12). The dates of the extreme values in the ring widths of the five older trees were relatively close to the timing of maximum MA, reflecting that the curve is more easily smoothed when averaged across a larger sample size.

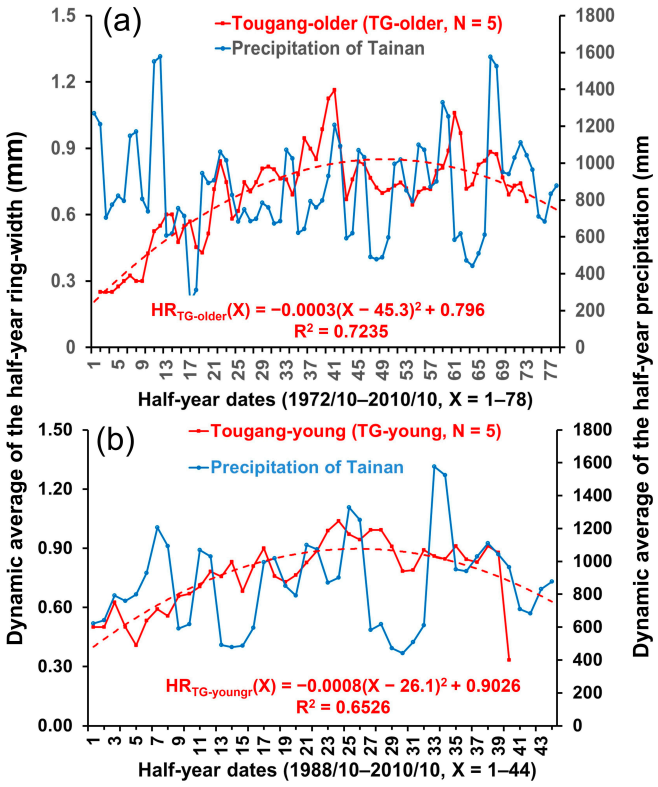


Figure 12. Dynamic average half-year ring widths used to estimate the time from prosperity to decline of mangrove trees at the Tougang Ditch (TG), Tainan City: (**a**) five order individuals; (**b**) five younger individuals. The 10 mangrove trees in TG experienced mortality during 2007 to 2009.

4. Discussion

Calculations based on 24 mangrove samples collected from the west coast of Taiwan revealed that the linear equation for annual radius growth was $R_{JS}(X) = 2.3705X - 4.5357$ ($R^2 = 0.9945$, X = 1–37). The slope of this equation is 90.5% of that reported by Fan, whose model was $R(X) = 2.618X + 1.9086$ [12].

4.1. Environmental Risk Factors ofLand Subsidence

Although the Zengwun Estuary Delta on the west coast of Taiwan has experienced slight subsidence due to tectonic activity, most western coastal areas have experienced severe land subsidence due to groundwater overpumping. Data from the land subsidence database of the Water Resources Agency indicate that the maximum cumulative subsidence in Taixi Township, Yunlin County, was approximately −283 cm, with an average annual subsidence of −5.9 cm (Table 1).

In some areas along Taiwan's west coast, severe land subsidence resulted from groundwater overpumping. From 1988 to 2009, the maximum cumulative subsidence in the Beimen area was approximately −94 cm, which explains why old mangrove trees at JS drowned and seedlings continued to expand inland. The correlation between changes in MA at Beimen and cumulative land subsidence highlighted a clear association between changes in MA at JS and land subsidence. By 2007, the MA at Beimen decreased to 17.35 ha.

Over the years, *A. marina* at TG exhibited a marked decline in annual ring width due to land subsidence. Notably, these trees still had green leaves before death, and many dead tree heads surrounded them. The radius growth of the outermost circle gradually decreased. In the present study, *A. marina* trees at JS and TG were assessed to generate the quadratic polynomial curve for declining carbon sink in land subsidence areas.

4.2. Estimation of Blue Carbon Content in Mangroves

The age of *A. marina* at TG was inferred by comparing the semiannual radius growth time series for dead mangroves with the semiannual rainfall time series from TN. This finding is consistent with the MA estimated derived from six aerial photographs and satellite images from 1975 to 2012 (Table 2). Accordingly, the time series trend equation for annual ring width, $Ysite(X) = -k(X - p)^2 + q$, and that for area, $MA_{site,area}(t) = -k(t - p)^2 + q$, can be applied to estimate the dynamic trend of mangrove carbon sinks in subsidence-affected areas (Appendix D). Furthermore, the trend line extrapolation method can be combined with previously reported values for carbon sequestration per unit area of mangrove forest to project future changes in MA and estimate blue carbon stocks.

Regarding the amount of blue carbon stored in mangroves growing in land subsidence areas, when cumulative land subsidence exceeds the height of their pneumatophores (PnRs, Figure 2) and seawater persistently submerges PnRs, mangrove growth begins to decline. After the parabolic trend reaches its vertex, the curve reverses, and the MA decreases. For a target year, carbon sequestration per unit area was estimated from studies providing relevant information per unit of MA [11,57].

In practical application, the annual ring width method requires careful, sequential steps.

1. Cut mangrove samples (subsample number > 4).
2. Measure annual ring width each year $YR_S(X)$, where X = 1, . . ., m.
3. Construct the time series $[YR_S(X)]$.
4. Fit the quadratic polynomial trend equation $YR_S(X) = -k(X - p)^2 + q$ to the time series.
5. Calculate the parabola vertex (p, q), where *p* is year and *q* is the maximum annual ring width (mm).

With the increasing availability of satellite imagery and area estimation techniques, the estimation method has become more feasible. We propose the following specific and feasible steps for estimating mangrove carbon sinks:

1. Obtain satellite images of the target area for estimating mangrove carbon sinks for 6 years (preferably with a gap between every 2 years) to extend the observation time axis.
2. Select the target sample area from ≥2 crossing lines (field surveys can be incorporated if necessary), ensuring each crossing line includes at least three fixed sample areas, with boundaries consistent across years and a total sample area exceeding 5 ha.
3. Apply Unsupervised Classification (Iso Cluster Unsupervised Classification) in ArcMap to estimate $MA_S(t)$, where t = 1, . . ., m, for each fixed sample area per year and construct the time series $[MA_S(t)]$.
4. Derive the quadratic polynomial trend equation for the time-series $MA_S(t)$ of the entire target area (or multiple sample sites): $MA_S(t) = -k(t - p)^2 + q$.

5. Calculate the vertex of the parabola (p, q), where *a* is the time and *b* is the maximum MA.

The carbon sequestration potential of *A. marina* is typically influenced by the tree age, seasonal variation, growth rate, and sediment characteristics. In addition, nutrient inputs from rainfall and the ecological effects of waterbird habitats also play a considerable role [30–34,73]. Reduced rainfall and groundwater extraction have led to land subsidence, which in turn diminished radial growth [4], indicating a sharp decline in net production. Rainfall exerts a dynamic influence throughout the year, whereas land subsidence imposes an irreversible impact. Lin et al. presented five carbon budgets for *A. marina* in the Asia–Pacific region (New Zealand, Indonesia, and Iran) and compared them with data from four sites in Taiwan [20,43,71,77,78].

The rate of land subsidence or water-level rise varies annually across different sample areas, making it impossible to determine mangrove tolerance to flooding duration or frequency from an average value (cm/year). Future research on *A. marina* carbon sequestration should first clarify whether subsidence has occurred at each study site and whether it influences the carbon budget and sequestration capacity of *A. marina*. Assessment methods based on small area and limited sample sizes of radial growth can accurately estimate growth status. Therefore, these methods can be applied to predict future carbon sinks, prevent misinterpretation of net productivity in subsidence-affected areas, the evaluation of *A. marina* carbon sinks in subsidence areas, and provide a practical basis for regulatory authorities to calculate and verify carbon sequestration.

Author Contributions: Conceptualization, F.-J.L. and Y.-T.U.; methodology, S.-H.C. and H.-Y.C.; software, C.-W.L. and Y.-T.U.; botany, K.-F.H.; validation, F.-J.L. and Y.-T.U.; formal analysis, Y.-T.U.; investigation, resources, writing and curation, F.-J.L. and Y.-T.U.; funding acquisition, F.-J.L. All authors have read and agreed to the published version of the manuscript.

Funding: Ocean Affairs Council, Ocean Conservation Administration, Taiwan (R.O.C.) Project Number: 114 Marine Conservation-0605-Biology-Geology-03, and 114 Marine Conservation-021-Biology-Geology-10.

Institutional Review Board Statement: Not applicable.

Informed Consent Statement: Not applicable.

Data Availability Statement: The mangrove data was collected by the participants, while other data was purchased from relevant government agencies.

Acknowledgments: We thank Jung-Ting Hsu, Bo-Wei Wang, Po-Ling Deng, Ching-Lung Liu, Yi-Ling Chen, and Meihua Landscape Engineering for helped with data collection and compilation. In addition, we thank Chia-Hung Jen, Chien-Jung Liu, Chih-Hua Chang, Kun-Neng Chen, Yu-Chen Lin, Zhan-Xian Zhan, Yu-Hwa Chen, Yun-Zhan Hsieh, Bo-Zhi Pan, Cheng-Hsun Yang, Feng-Tse Yang, and Ha-Xiang Yang for their assistance with fieldwork and data collection. This study was facilitated by the Ocean Conservation Administration, Ocean Affairs Council, Construction and Planning Agency, Ministry of the Interior, Fourth River Management Branch, Chiayi County Government, and Tainan City Government.

Conflicts of Interest: The authors declare no relevant conflicts of interest.

Abbreviations

The following abbreviations are used in this manuscript:

BD	Budai Lagoon
CG	Cigu Fishpond
DS	Dongshih Lagoon
HG	half-year radius growth

HM Haomeiliao Wetland
JJ Jiangjyun River
JS Jishui Estuary
MA mangrove area
PL linear rainfall equation
PZ′ Puzih Estuary
SC Sihcao Wetland
SJ Syuejia Wetalnd
TG Tougang Ditch
TL linear temperature equation
TN Former Tainan Meteorological Station
YR annual ring width

Appendix A. Historical Mangrove Planting at Cigu Lagoon, Tainan City (1963–1964), but Later Removed and Buried Due to Salt Pan Development, in 1971

Table A1. Number and locations of mangrove species planted by forestry authorities at Cigu Lagoon, Tainan City, in 1963–1964, according to Chang's (1970) report [47].

Scientific Name	Seedling Collection Site	Individuals	Planting Location (Tainan City)
Kandelia obovata	Tamsui, Taipei	1,030,000	Qinkunshen and Xiliao
Avicennia marina	Southern Taiwan	600,000	Qinkunshen Xiliao
Rhizophora mucronata	Tainan City	40,600	Qinkunshen, Xiliao
Sonneratia alba	Vietnam	300,000	Xiliao
Avicennia officinalis	Vietnam	90	Xiliao
Sonneratia caseolaris	Vietnam	17	Xiliao
Avicennia marina	Vietnam	27	Xiliao
Rhizophora conjugata	Vietnam	10	Xiliao
	Total	2,293,037	

Appendix B. Changes in Mangrove Area at Dongshih Lagoon (DS), Budai Lagoon (BD), Jshui Estuary (JS), and Tougang Ditch (TG), West Taiwan (1975–2012)

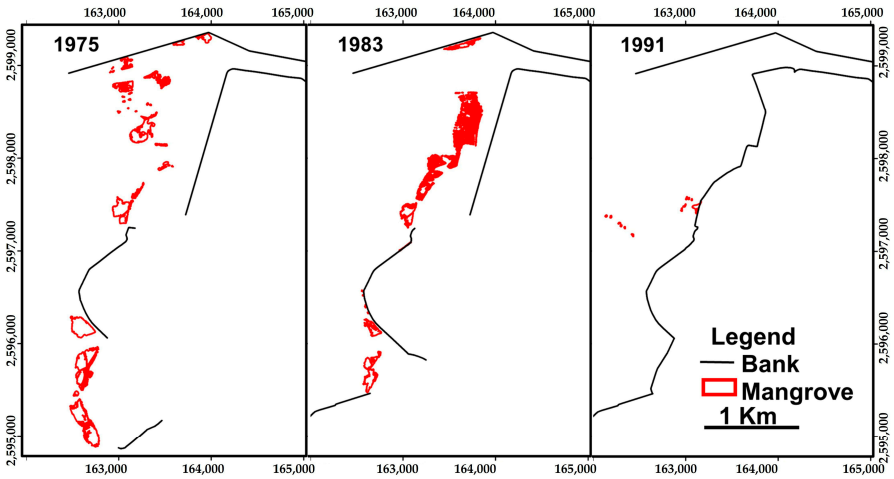


Figure A1. Changes in mangrove area at Dongshih Lagoon (DS), Chiayi County (1975–1991). After 1975, extensive mangrove stands developed due to siltation from the Waisanding Sand Bar and Beigang River. Following rapid land subsidence after 1983, mangroves declined sharply, shrinking to only 0.6 ha by 1991.

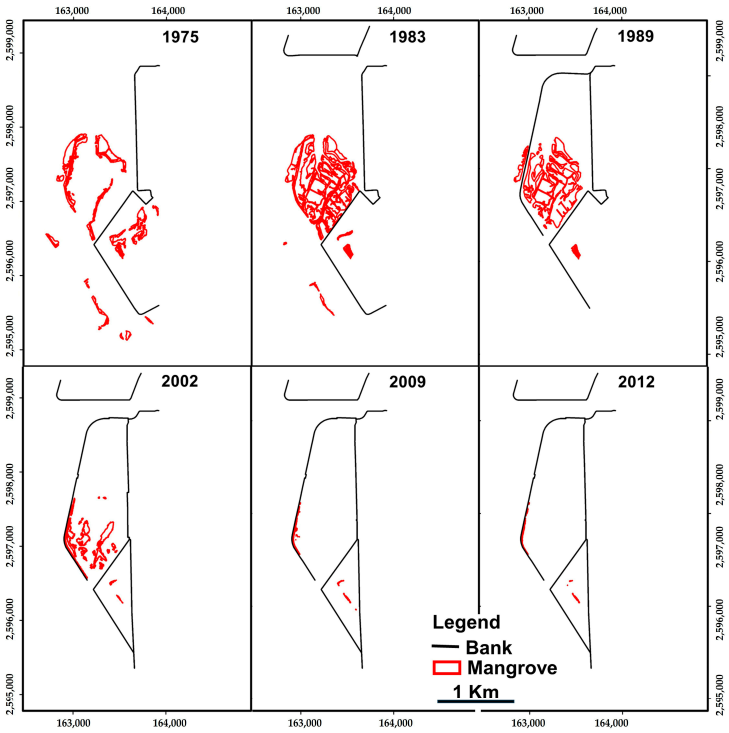


Figure A2. Changes in mangrove area at Budai Lagoon (BD), Chiayi County (1975–2012). After 1975, significant siltation led to the formation of extensive mangrove forests. However, following rapid land subsidence after 1983, these forests gradually declined and eventually died out.

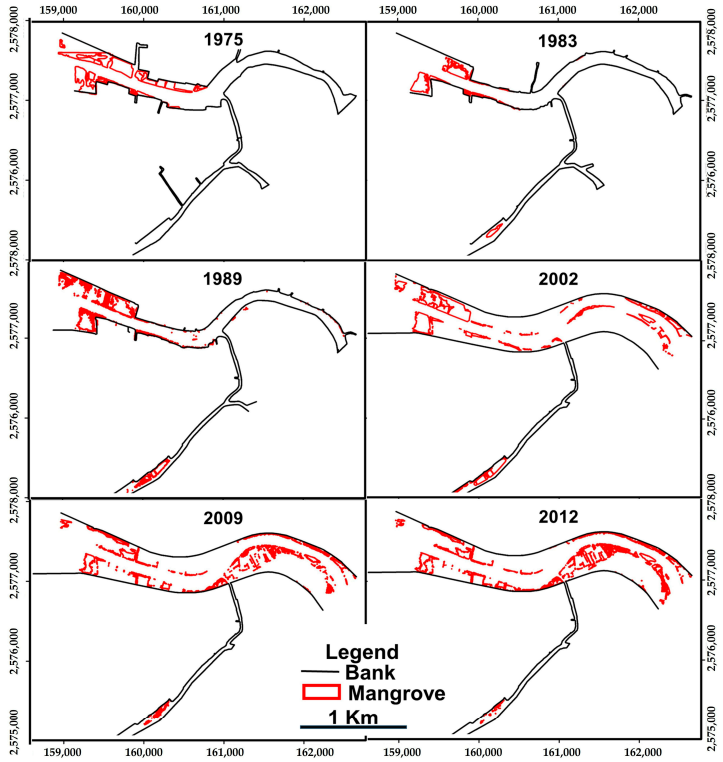


Figure A3. Changes in mangrove areas at Jishui Estuary (JS) and Tougang Ditch (TG), Tainan City (1975–2012). At the estuary within the subsidence zone, mangroves near the river mouth gradually declined. Meanwhile, new stands progressively expanded upstream, reflecting a spatial shift in mangrove distribution under subsidence conditions.

Appendix C. Extreme Values and Peaks of a Quadratic Parabola

In the maps of 1975 and 1983, horsetail trees (*Casuarina* sp.), fishponds, dry fields, and rice fields were marked along the beach, estuary, and riverside. The term "mangroves" first appeared in maps of 1989, where early identification relied on vegetation near the waterline. MAs were depicted individually based on their ability to withstand high and low tides [68]. The orthoimage digital files purchased from the Agricultural and Forestry Aerial Survey Institute contained TWD97 coordinates, with resolutions of 0.5×0.5 m^2 in 2002 and 0.25×0.25 m^2 from 2009 onward. The high-resolution datasets facilitated the identification and depiction of individual mangroves in river channels. In 2017, SPOT-7 satellite images were purchased from the Center for Space Remote Sensing Research at National Central University. These images contained TWD97 coordinates, had a resolution of 1.5×1.5 m^2, and provided red–green–blue plus near-infrared bands. Mangrove vegetation in high- and low-tidal areas was identified using the Iso Cluster Unsupervised Classification function in ArcMap. Owing to the low resolution, distinguishing very small patches was challenging. Upstream areas of Jishui Creek contained mixed vegetation comprising mangroves, mixed forest, and crops. Because these areas formed relatively recently, corrections were made after onsite inspection and comparison.

Satellite images obtained from the Center for Space and Remote Sensing Research included one SPOT-7 image acquired on 22 March 2017 (Center for Space and Remote Sensing Research 2024). These images were used to estimate mangrove coverage within the study sites. As mentioned, the JS site was divided into seven subsites (JS-A to JS-G) (Figures 2 and 3) to separate areas affected by the restoration project. The MA of each subsite between 1975 and 2012 was calculated.

Two onsite surveys were conducted in December 2014 and August 2023. The results revealed only a few *K. obovata* and *A. marina* scattered along the riverside approximately 300 m upstream of the Puzi River Port Bridge in Chiayi County. Notably, because of the low plant count, small area, strip-shaped patches, and mixed growth with agarwood and bitterwood shrubs, the SPOT-7 satellite image from 22 March 2017 was difficult to interpret. Therefore, the area upstream of the Port Bridge was excluded from analysis [71].

Appendix D. Extreme Values and Peaks of a Quadratic Parabola

The growth status of mangroves in the land subsidence area changes from vigorous to declining, and the quadratic trend line of their annual ring width time series shows a downward bend. The quadratic trend line is expressed as

$$YR(X) = aX^2 + bX + c \quad \text{(A1)}$$

where a, b, and c are constants, and X denotes the years. A negative value of a indicates land subsidence, whereas a positive value of a suggests no land subsidence or minimal subsidence.

After calculation and rearrangement, the equation can be written as

$$YR(X) = -k(X - p)^2 + q \quad \text{(A2)}$$

where k, p, and q are constants, and X denotes the year. A negative value of $-$k indicated severe land subsidence, with the extremum q (mm/year) occurring in year p. In addition, $p = b/(2a)$, $q = a(p^2) + c$. The coordinates (p, q) represent the vertex of the quadratic parabola, corresponding to the highest point of the trend line. Furthermore, $-2k$ denotes the annual ring width deceleration rate.

References

1. Central Weather Administration. Precipitation and Temperature Data. Available online: https://www.cwa.gov.tw/eng/ (accessed on 1 March 2025).
2. Jaramillo, F.; Licero, L.; Åhlen, I.; Manzoni, S.; Rodríguez-Rodríguez, J.A.; Guittard, A.; Hylin, A.; Bolaños, J.; Jawitz, J.; Wdowinski, S.; et al. Effects of hydroclimatic change and rehabilitation activities on salinity and mangroves in the Cienaga Grande de Santa Marta, Colombia. *Wetlands* **2018**, *38*, 755–767. [CrossRef]
3. Rahaman, S.M.B.; Sarder, L.; Rahaman, S.M.B.; Ghosh, A.K.; Biswas, S.K.; Siraj, S.S.; Huq, K.A.; Hasanuzzaman, A.F.M.; Islam, S.S. Nutrient dynamics in the Sundarbans mangrove estuarine system of Bangladesh under different weather and tidal cycles. *Ecol. Process.* **2013**, *2*, 29. [CrossRef]
4. Chang, S.-H. The Effects of Land-Subsidence on the Mangrove Ecosystems: A Case Study of Jishui Estuary and Pujsu River. Master's Thesis, Department of Environmental Engineering, Kun Shan University, Tainan City, Taiwan, 2012.
5. Menezes, M.; Berger, U.; Worbes, M. Annual growth rings and long-term growth patterns of mangrove trees from the Bragança peninsula, North Brazil. *Wetl. Ecol. Manag.* **2003**, *11*, 233–242. [CrossRef]
6. Villate Daza, D.A.; Moreno, H.S.; Portz, L.; Manzolli, R.P.; Bolívar-Anillo, H.J.; Anfuso, G. Mangrove forests fvolution and threats in the Caribbean Sea of Colombia. *Water* **2020**, *12*, 1113. [CrossRef]
7. Gagnon, J.D. Rainfall and the width of annual rings in planted white spruce. *For. Chron.* **1961**, *37*, 96–101. [CrossRef]
8. Casal, G.; Tregarot, F.; Cornet, C.C.; McCarthy, T.; van der Gees, M. A cost-effective method to map mangrove forest extent, composition, and condition in small islands based on Sentinel-2 data: Implications for management. *Ecol. Indic.* **2024**, *159*, 111696. [CrossRef]
9. Kandasamy, K.; Bingham, B.L. Biology of mangroves and mangrove ecosystems. *Adv. Mar. Biol.* **2001**, *40*, 81–251. [CrossRef]
10. Purnobasuki, H. Characteristics of root caps in four root types of *Avicennia marina* (Forsk.) Vierh. *Am. J. Plant Sci.* **2013**, *4*, 853–858. [CrossRef]
11. Lin, H.-J.; Chen, K.-Y.; Kao, Y.-C.; Lin, W.-J.; Lin, C.-W.; Ho, C.-W. Assessing coastal blue carbon sinks in Taiwan. *J. Mar. Res.* **2023**, *3*, 1–17. [CrossRef]
12. Fan, K.-C. Litterfall and nutrient dynamics of a mangrove *Avicennia marina* (Forsk.) Vierh. Forest at the Chishui River, Tainan County, Taiwan. *Taiwan J. For. Sci.* **2007**, *22*, 441–454. [CrossRef]
13. Igulu, M.M.; Nagelkerken, I.; van der Velde, G.; Mgay, Y.D. Mangrove fish production is largely euelled by external food sources: A stable Isotope analysis of fishes at the individual, species, and community levels from across the globe. *Ecosystems* **2013**, *16*, 1336–1352. [CrossRef]
14. Ueng, Y.-T.; Wang, Y.-K.; Tsao, C.-W.; Tung, S.-C.; Hsu, J.-T.; Chang, Y. Monitoring and assessment of oyster and barnacle larvae settlement in an oyster farm in western Taiwan. *Nat. Resour.* **2020**, *11*, 112–126. [CrossRef]
15. Ueng, Y.-T.; Lin, F.-J.; Tsao, C.-W.; Chen, H.-C.; Chang, W.-C. Sand grain size and organic matter in the intertidal zone on the Southwest Taiwan Coast. *Nat. Resour.* **2021**, *12*, 108–123. [CrossRef]
16. Lin, H.-J.; Kao, W.-Y.; Wang, Y.-T. Analyses of stomach contents and stable isotopes reveal food sources of estuarine detritivorous fish in tropical/subtropical Taiwan. *Estuar. Coast. Shelf S* **2007**, *73*, 527–537. [CrossRef]
17. Nagelkerken, I.; Blaber, S.J.M.; Bouillon, S.; Green, P.; Haywood, M.; Kirton, L.G.; Meynecke, J.O.; Pawlik, J.; Penrose, H.M.; Sasekumr, A.; et al. The habitat function of mangroves for terrestrial and marine fauna: A review. *Aquat. Bot.* **2008**, *89*, 155–185. [CrossRef]
18. da Silva, F.R.M.; Filho, E.M.N.; Gallina, M.L.; Keppeler, F.W.; Loiola, M.; Giarrizzo, T. From fisher tales to scientific evidence: Revealing the significance of estuarine and mangrove habitats as nursery grounds for juveniles of the largest Atlantic Ocean snapper. *Front. Mar. Sci.* **2023**, *10*, 1292788. [CrossRef]
19. Hsueh, M.-L. *Disappearing Wetland Forests: Taiwan's Mangroves; Conservation Education Center*; Endemic Species Research Institute, C.O.A.: Nantou County, Taiwan, 1995.
20. Swales, A.; Denys, P.; Pickett, V.I.; Lovelock, C.E. Evaluating deep subsidence in a rapidly-accreting mangrove forest using GPS monitoring of surface-elevation benchmarks and sedimentary records. *Mar. Geol.* **2016**, *380*, 205–218. [CrossRef]
21. Xu, S.; Chen, Z.; Li, S. The habitat functions of mangroves for aquatic fauna and fisheries. *Acta Ecol. Sin.* **2010**, *30*, 186–196.
22. Savage, C.; Thrush, S.F.; Lohrer, A.M.; Hewitt, J.E. Ecosystem services transcend boundaries: Estuaries provide resource subsidies and influence functional diversity in coastal benthic communities. *PLoS ONE* **2012**, *7*, e42708. [CrossRef] [PubMed]
23. Whitfield, A.K.; Able, K.W.; Blaber, S.J.M.; Elliott, M.; Franco, A.; Harrison, T.D.; Houde, F.D. Feeding ecology and trophic dynamics. In *Fish and Fisheries in Estuaries: A Global Perspective*; Whitfield, A.K., Able, K.W., Blaber, S.J.M., Elliott, M., Eds.; John Wiley & Sons Ltd: New York, NY, USA, 2012; pp. 255–331. [CrossRef]
24. Zhao, J.; Li, C.; Wang, T.; Li, C.; Shen, J.; Liu, Y.; Wu, P. Distribution pattern of mangrove fish communities in Chin. *Biology* **2022**, *11*, 1696. [CrossRef]
25. Hsueh, M.-L.; Lee, H.-H. Diversity and distribution of the mangrove forests in Taiwan. *Wetl. Ecol. Manag.* **2000**, *8*, 233–242. [CrossRef]

26. Ueng, Y.-T.; Lin, K.-H. (Eds.) *Demonstration Planning for Protected Areas in Environmentally Sensitive Zones in Taiwan's Coastal Areas—Report on the Results of Bird, Mangrove, and Wetland Survey Projects*; Taiwan Wetland Conservation Alliance: Kaohsiung City, Taiwan, 1994.
27. Wang, H.-U.; Fu, S.-W.; Deng, G.-Z.; Hong, X.-Z.; Liao, X.-Y. Changes in mangrove area and species composition in Taiwan. *Taiwan J. For. Sci.* **2015**, *41*, 41–57. Available online: https://www.forest.gov.tw/0000104/0000497 (accessed on 1 February 2025).
28. Sheue, C.-R.; Liu, H.-Y.; Yong, J.W.H. *Kandelia obovata* (Rhizophoraceae), a new mangrove species from Eastern Asia. *Taxon* **2003**, *52*, 287–294. [CrossRef]
29. Ueng, Y.-T.; Wang, J.-P. A new species of the Genus *Fronsella* (Mollusca: Montacutidae) from Taiwan. *J. Natl. Taiwan Mus.* **2005**, *58*, 93–99.
30. Weng, J.-H.; Ueng, Y.-T. First report on the breeding of great white egret (*Egretta alba*) in Southwesten Taiwan. *J. Natl. Taiwan Mus.* **2005**, *58*, 59–67.
31. Weng, R.X.; Weng, Y.C.; Wang, J.P.; Peng, R.J. The breeding of intermediate egret (*Egretta intermedia*) in Southwestern Taiwan. *Wild Birds* **2004**, *8*, 69–73, 89–90.
32. Yang, J.Y.-C.; Ueng, Y.-T. *Taiwan's Wetlands of Importance*; Urban and Rural Development Branch, Construction and Planning Agency, Ministry of the Interior: Taipei, Taiwan, 2011; p. 32.
33. Yen, L.-F. Diet Analysis of Five Herons in Tainan. Master's Thesis, Department of Life Sciences National Cheng Kung University, Tainan City, Taiwan, 2014.
34. Chen, T.-H. A Study on the Spiders Cluster of Mangrove in Jishuei River and Puzih River, Taiwan. Master's Thesis, Department of Environmental Engineering, Kun Shan University, Tainan City, Taiwan, 2019.
35. Liao, C.-H.; Ueng, Y.T. The report of population distribution and captive-bred of Long-legged flies *Thinophilus* (Diptera: Dolichopodidae) in Jishui Estuary of Taiwan. *Wetl. Taiwan* **2019**, *8*, 65–76.
36. Wu, T.-H. Forest management and carbon storage. *J. For. Res.* **2009**, *16*, 47–55.
37. Wu, H.-H. The Carbon Budgets of *Kandelia obovata* and *Avicennia marina* Mangroves. Master's Thesis, Department of Life Sciences, National Chung Hsing University, Taichung, Taiwan, 2021.
38. Ueng, Y.-T.; Lin, F.-J.; Hsiao, Y.-W.; Chen, P.-S. A new carbon sinks and biodiversity-weighted model—A case study on the coastal wetlands of Southwest Taiwan. *Wetl. Sci. Pract.* **2025**, *43*, 17.
39. Ueng, Y.-T.; Lin, F.-J.; Hsiao, Y.-W.; Chen, P.-S.; Chang, H.-Y. Overemphasis on blue carbon leads to biodiversity loss: A case study on subsidence coastal wetlands in Southwest Taiwan. *J. Bus. Econ. Stat.* **2025**, *27*, 46–57. [CrossRef]
40. Rateb, A.; Abotalib, A.Z. Inferencing the land-subsidence in the Nile Delta using Sentinel-1 satellites and GPS between 2015 and 2019. *Sci. Total Environ.* **2020**, *729*, 138868. [CrossRef]
41. Wu, P.-C.; Wei, M.M.; D'Hondt, S. Subsidence in coastal cities throughout the world observed by InSAR. *Geophys. Res. Lett.* **2022**, *49*, e2022GL098477. [CrossRef]
42. Pedretti, L.; Giarola, A.; Korff, M.; Lambert, J.; Meisina, C. Comprehensive database of land-subsidence in 143 major coastal cities around the world: Overview of issues, causes, and future challenges. *Front. Earth Sci.* **2024**, *12*, 1351581. [CrossRef]
43. Riastama, C.N.; Anjasmara, I.M.; Maulida, P. Monitoring land-subsidence and its effect on Surabaya coastal inundation by utilizing GPS campaigns data. *Earth Environ. Sci.* **2023**, *1127*, 012002. [CrossRef]
44. Sun, H.; Peng, H.; Zeng, M.; Wang, S.; Pan, Y.; Pi, P.; Xue, Z.; Zhao, X.; Zhang, A.; Liu, F. Land-subsidence in a coastal city based on SBAS-InSAR monitoring: A case study of Zhuhai, China. *Remote Sens.* **2023**, *15*, 2424. [CrossRef]
45. Mao, G.-G. A study on the preventing strategies of aquifer subsidence at Pingtung coastal area. *Rural Dev.* **2002**, *3*, 35–58.
46. Water Resources Agency. Land Subsidence Monitoring Information Integration Service System. Available online: https://web.wra.gov.tw/landsubsidence/water_new/Home/IndexReNew (accessed on 1 December 2024).
47. Chang, S.-T. Mangroves in Taiwan and their function of promoting new land. *Bank Taiwan Q.* **1970**, *21*, 82–110.
48. Shih, H.-T.; Sheue, C.-R.; Yang, Y.-P. Changes in the distribution of Mangroves in Taiwan. *J. Natl. Taiwan Mus.* **2025**, *78*, 1–38. [CrossRef]
49. Chen, Y.-C. The Study of Mangrove Distribution Change on Tonshu, Chiayi County. Master's Thesis, The Graduate Institute of Geography, National Taiwan University, Taipei City, Taiwan, 2001.
50. Clunie, N.M.U. Death of mangroves: Upper Whangarei harbour. In *Conservation Advisory Science Notes No. 32*; Department of Conservation: Wellington, New Zealand, 1993.
51. Shen, C.-C. Current status and conservation of Taiwan mangroves. *Taiwan Mus.* **1993**, *12*, 22–25.
52. Water Resources Agency, MOEA. *Land-Subsidence Information*; Water Resources Agency, MOEA: Taichung, Taiwan, 2024.
53. Water Resources Agency, MOEA. *The Jishui River System and Its Tributary, the Baishui River, Are Under Management*; Water Resources Agency, MOEA: Taichung, Taiwan, 2017. Available online: https://www.wra.gov.tw/cl.aspx?n=3527 (accessed on 1 February 2025).
54. Sunkur, R.; Kantamaneni, K.; Bokhoree, C.; Rathnayake, U.; Fernando, M. Mangrove mapping and monitoring using remote sensing techniques towards climate change resilience. *Sci. Rep.* **2024**, *14*, 6949. [CrossRef]

55. Fathah, A.L.; Semedi, B.; Wardana, F.C.; Isdianto, A. Assessment of mangrove diversity, biomass, and carbon stocksin the Ujungpangkah Estuary. *Gresik. J. Environ. Eng. Sustain. Technol.* **2025**, *12*, 25–34.
56. Whilst NIWA. *Coastal Hazards and Sea-Level Rise in Wellington City Supporting the 2020–2021 District Plan Process Prepared for Wellington City Council*; NIWA Client Report; Whilst NIWA: Auckland, New Zealand, 2021.
57. Lin, W.-J.; Lin, C.-W.; Wu, H.-H.; Kao, Y.-C.; Lin, H.-J. Mangrove carbon budgets suggest the estimation of net production and carbon burial by quantifying litterfall. *CATENA* **2023**, *232*, 107421. [CrossRef]
58. Huang, J.-Z. An Estimation of Carbon Fixation Capacity in Mangrove Forest Taijiang National Park. Master's Thesis, Forestry and Natural Resources Department of National Chiayi University, Chiayi City, Taiwan, 2012.
59. Li, S.-B. Carbon Budget of Mangroves in the Chiku Area, Tainan. Master's Thesis, Department of Life Sciences, National Chung Hsing University, Taichung, Taiwan, 2015.
60. Thotli, L.R.; Gugamsetty, B.; Kalluri, R.O.R.; Tandule, C.R.; Kotalo, R.G.; Akkiraju, B.; Lingala, S.S.R. Long-term (2001–2020) trend analysis of temperature and rainfall and drought characteristics by in situ measurements at a tropical semi-arid station from southern peninsular India. *Int. J. Climatol.* **2022**, *42*, 8928–8949. [CrossRef]
61. Kamp, J.; Frank, C.; Trautmann, S.; Busch, M.; Flade, M.; Gerlach, B.; Karthäuser, J.; Kunz, F.; Mitschke, A.; Schwarz, J.; et al. Population trends of common breeding birds in Germany 1990–2018. *J. Ornithol.* **2020**, *162*, 1–15. [CrossRef]
62. Chen, P.-S.; Chei, S.-J.; Kuo, T.-H.; Deng, P.-L.; Liu, C.-L.; Ueng, Y.-T. Population growth, habitat use, and conservation strategies of the Black-faced Spoonbill (*Platalea minor*) in the southwest coast of Taiwan. *Wilson J. Ornithol.* **2024**, *135*, 492–501. [CrossRef]
63. van Bijsterveldt, C.E.J.; Herman, P.M.J.; van Wesenbeeck, B.K.; Ramadhani, S.; Heuts, T.S.; van Starrenburg, C.; Tas, S.A.J.; Triyanti, A.; Helmi, M.; Femke, H.; et al. Subsidence reveals potential impacts of future sea level rise on inhabited mangrove coasts. *Nat. Sustain.* **2023**, *6*, 1565–1577. [CrossRef]
64. Lee, M.-Y. Causes of the hundred-year drought in Taiwan in 2020/21. *Conf. Disaster Manage. Taiwan* **2021**, *202*, 141–144. [CrossRef]
65. Weiskopf, S.R.; Lerman, S.B.; Isbell, F.; Morelli, T.L. Biodiversity promotes urban ecosystem functioning. *Ecography* **2024**, *2024*, e07366. [CrossRef]
66. Law, M.; Collins, A. *Getting to Know Arcgis Desktop 10.8*; Esri Press: Redlands, CA, USA, 2022.
67. Krebs, C.J. *Ecological Methodology*, 2nd ed.; Benjamin/Cummings: Menlo Park, CA, USA, 1999.
68. Chen, P.-S.; Chei, S.-J.; Kuo, T.-H.; Deng, P.-L.; Liu, C.-L.; Ueng, Y.-T. Water bird communities in nonoperational Cigu salt pan wetland of varying land elevation and water depth on the Southwest Taiwan coast. *Nat. Resour.* **2020**, *11*, 20–37. [CrossRef]
69. Moore, I.D.; Grayson, R.B.; Ladson, A.R. Digital Terrain Modelling: A review of hydrological, geomorphological, and biological applications. *Hydrol. Process.* **1999**, *5*, 3–30. [CrossRef]
70. Tarboton, D.G. A New method for the determination of flow directions and upslope areas in grid digital elevation models. *Water Resour. Res.* **1997**, *33*, 309–319. [CrossRef]
71. Febriandi, F. The estimation of mangroves area and density of mangroves changes use the remote sensing data at Northheast Province of Aceh, Indonesia. *Sumatra J. Disaster Geogr. Geogr. Educ.* **2017**, *1*, 105–110. [CrossRef]
72. Benson, L.V.; Petersen, K.; Stein, J. Anasazi (pre-Columbian Native-American) migrations during the middle-12th and late-13th centuries–were they drought induced? *Clim. Change* **2007**, *83*, 187–213. [CrossRef]
73. Chang, Y.-S. Using Tree Ring Stable Oxygen Isotope to Reconstruct Historical Climates in Taijiang Inland Sea in Taiwan. Master's Thesis, Department of Life Sciences National Cheng Kung University, Tainan, Taiwan, 2020.
74. Yang, P.-C. Relative Contribution of Plant- and Animal-Derived Detritus in Riverine and Fringe Mngroves in Taiwan. Master's Thesis, Department of Bioenvironmental Systems Engineering, National Taiwan University, Taipei, Taiwan, 2021.
75. Huang, J.-S. Effects of Thinning on Carbon Sequestration in Mangroves. Master's Thesis, Department of Life Sciences, National Chung Hsing University, Taichung, Taiwan, 2016.
76. El-Hussieny, S.A.; Kamal, H.; Shaltout, K.H.; Alatar, A.A. Carbon sequestration potential of *Avicennia marina* (Forssk.) Vierh. and *Rhizophora mucronata* Lam. along the Western Red Sea Coast of Egypt. *Rend. Lincei-Sci. Fis.* **2021**, *32*, 599–607.73. [CrossRef]
77. Duke, N.C.; Birch, W.R.; Williams, W.T. Growth rings and rainfall correlations in a mangrove tree of the genus *Diospyros* (Ebenaceae). *Aust. J. Bot.* **1981**, *29*, 135–142. [CrossRef]
78. Nguyen, H.T.; Stanton, D.E.; Schmitz, N.; Farquhar, G.D.; Bal, M.C. Growth responses of the mangrove *Avicennia marina* to salinity: Development and function of shoot hydraulic systems require saline conditions. *Ann. Bot.* **2015**, *15*, 397–407. [CrossRef]

Disclaimer/Publisher's Note: The statements, opinions and data contained in all publications are solely those of the individual author(s) and contributor(s) and not of MDPI and/or the editor(s). MDPI and/or the editor(s) disclaim responsibility for any injury to people or property resulting from any ideas, methods, instructions or products referred to in the content.